Vascular reactivity in small cerebral perforating arteries with 7 T phase contrast MRI – A proof of concept study

Lennart J. Geurts [a,*], Alex A. Bhogal [a], Jeroen C.W. Siero [a,b], Peter R. Luijten [a], Geert Jan Biessels [c], Jaco J.M. Zwanenburg [a]

[a] Department of Radiology, University Medical Center Utrecht, Utrecht, The Netherlands
[b] Spinoza Centre for Neuroimaging Amsterdam, Amsterdam, The Netherlands
[c] Department of Neurology and Neurosurgery, Brain Centre Rudolf Magnus, University Medical Center Utrecht, Utrecht, The Netherlands

A B S T R A C T

Existing cerebrovascular reactivity (CVR) techniques assess flow reactivity in either the largest cerebral vessels or at the level of the parenchyma. We examined the ability of 2D phase contrast MRI at 7 T to measure CVR in small cerebral perforating arteries.

Blood flow velocity in perforators was measured in 10 healthy volunteers (mean age 26 years) using a 7 T MR scanner, using phase contrast acquisitions in the semioval center (CSO), the basal ganglia (BG) and the middle cerebral artery (MCA). Changes in flow velocity in response to a hypercapnic breathing challenge were assessed, and expressed as the percentual increase of flow velocity as a function of the increase in end tidal partial pressure of CO_2.

The hypercapnic challenge increased (fit $\pm$ standard error) flow velocity by $0.7 \pm 0.3\%$/mmHg in the CSO ($P < 0.01$). Moreover, the number of detected perforators (mean [range]) increased from 63 [27–88] to 108 [61–178] ($P < 0.001$). In the BG, the hypercapnic challenge increased flow velocity by $1.6 \pm 0.5\%$/mmHg ($P < 0.001$), and the number of detected perforators increased from 48 [24–66] to 63 [32–91] ($P < 0.01$). The flow in the MCA increased by $5.2 \pm 1.4\%$/mmHg ($P < 0.01$).

Small vessel specific reactivity can now be measured in perforators of the CSO and BG, using 2D phase contrast at 7 T.

Introduction

With the increased SNR available in ultra-high field strength MRI, it has become feasible to measure increasingly smaller anatomical structures and their function in vivo. Recently, we developed a 2D phase contrast method at 7 T MRI, capable of measuring the time resolved blood flow velocity and pulsatility index in cerebral perforating arteries with diameters between 10 and 300 μm (Bouvy et al., 2016; Geurts et al., 2018). Abnormalities in these perforators, also referred to as cerebral small vessel disease (SVD), are a major cause of stroke and dementia (Pantoni, 2010; Wardlaw et al., 2013). Measuring hemodynamic properties of these small perforators may help to unravel the

pathophysiological processes of SVD (Broderick et al., 1997; Lee et al., 2007; Mitchell, 2008; Mitchell et al., 2011).

A hemodynamic property that is relevant, is cerebrovascular reactivity (CVR). CVR is a physiological mechanism that contributes to cerebral autoregulation. To influence resistance and flow, vessel diameters change with perfusion pressure variation, but also with arterial CO_2 levels. Impaired CVR has been linked to white matter hyper-intensities, vascular dementia and an increased risk of stroke by a growing body of literature (Beishon et al., 2017; Reinhard et al., 2014; Reuck et al., 1999; Sam et al., 2016a, 2016b). CVR can currently be measured on a tissue level using blood oxygenation level dependent (BOLD) MRI, arterial spin labeling (ASL) or positron emission tomography (Halani et al., 2015;

Heijtel et al., 2014). CVR can also be measured at the level of the large intracranial arteries via Transcranial Doppler ultrasound (TCD) or phase contrast MRI (Leung et al., 2013). Currently there are no established methods to non-invasively assess reactivity in small arteries that are situated in between the large arteries and the tissue. Bridging this gap may help characterize reactivity in the cerebral vascular system as a whole. Now that 2D phase contrast MRI at 7 T can reliably measure blood flow velocity in perforators, it might be possible that it can also measure CVR in these small vessels (Geurts et al., 2018). Measuring CVR in perforating arteries with 2D phase contrast would complement existing methods and can help to pinpoint CVR impairments directly associated with local ischemia.

The aim of this paper is to determine whether it is feasible to measure CVR with the previously developed 2D phase contrast method in the cerebral perforating arteries of the semioval center and the basal ganglia. As a reference, we perform the same measurement in the middle cerebral artery as well. In all three experiments a baseline measurement was acquired, followed by a measurement in which the partial pressure of end tidal CO_2 (PetCO$_2$) was increased using a computer controlled gas delivery system. The change in blood flow velocity was taken as the primary outcome. Since increased blood flow increases blood signal through the T1-inflow effect, it becomes more likely that perforators are detected during the challenge (Bhogal et al., 2014; Brown et al., 2014; Geurts et al., 2018). Therefore, the change in number of detected perforators was taken as the secondary outcome. Systematic errors of CVR of the perforating arteries were qualitatively assessed through simulation.
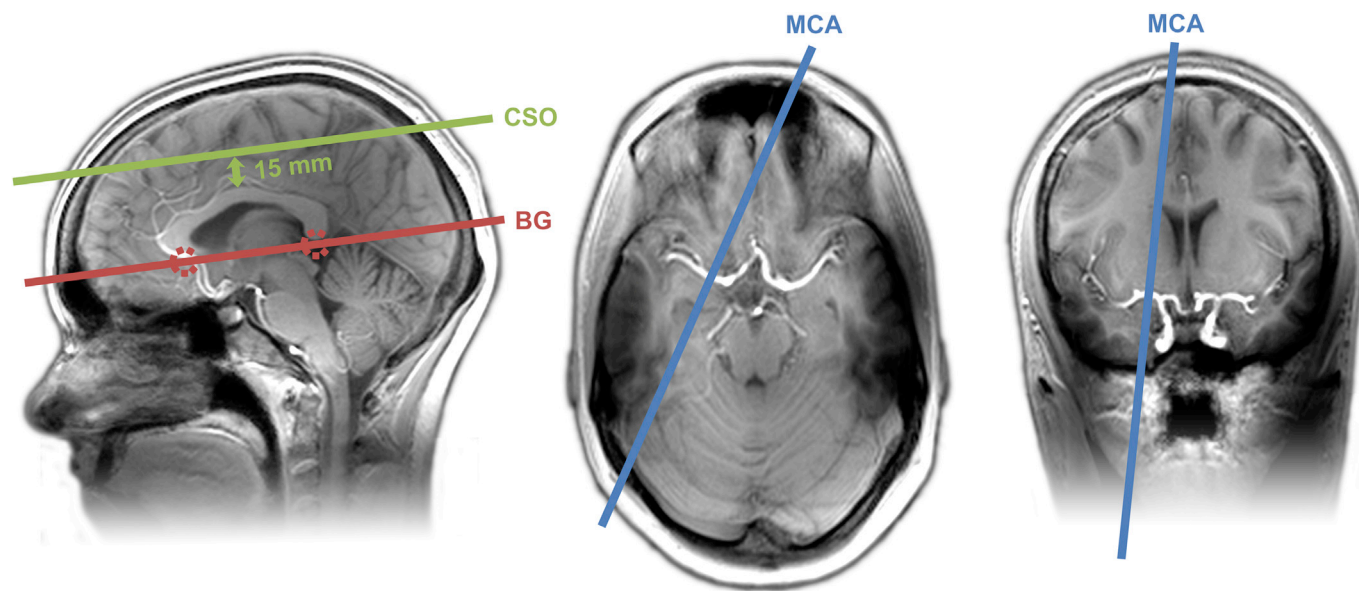
Methods

Data acquisition

A group of 10 healthy volunteers was scanned using a 7 T MRI system (Philips Healthcare, Best, The Netherlands) and a 32 channel receive coil with volume T/R transmit coil (Nova Medical, Wilmington, MA, USA). The institutional review board of our hospital approved this study and all subjects provided written informed consent. A 2D phase contrast acquisition was performed at three anatomical locations during baseline breathing and hypercapnia. The phase contrast acquisitions were alternated with T1 weighted 3D turbo field echo (T1w) acquisitions for white

matter segmentation. Interleaving structural scans with hypercapnic scans provided subjects with a rest period in which CO_2 values could fully return to resting values for subsequent baseline phase contrast scans. Baseline acquisitions were only started when CO_2 values had returned to normal. These scans also avoided potential problems due to (slight) changes in subject position over the duration of the exam, which would result in problems aligning the white matter segmentation with the 2D phase contrast results.

The planning of the three phase contrast slices is shown in Fig. 1. One slice was acquired in the perforating arteries of the semi-oval center (CSO, the white matter core underneath the cortical grey matter). The CSO contains perforators with very small diameters (10–300 μm), branching off from pial arteries. These perforators feed the capillary network of the white matter, the CVR of which is an area of active study (Sam et al., 2016a, 2016b). A group of larger perforators (diameters up to 1 mm) were measured with another phase contrast slice in the basal ganglia (BG, the subcortical nuclei of grey matter at the base of the brain). Their larger size ensures a higher blood signal and lower partial volume effect. The middle cerebral artery (MCA, the largest of the major arteries of the brain) was measured as a large reference vessel with known reactivity (Leung et al., 2013; Valdueza et al., 1999; Verbree et al., 2014). A phase contrast acquisition was performed in the MCA on one side, taking the side that allowed the most ease in planning (long straight segment without major branches).

The CSO acquisitions were performed first. To have a large number of successful reference measurements, the MCA acquisitions were acquired second. The BG acquisitions were performed last in the protocol, since these perforators, with intermediate diameters, were the least critical for answering the research question. If an acquisition showed excessive motion artifacts, it was performed again after the standard protocol, but only if the subject was still comfortable and within a maximum of 1 h of scanning.

All acquisition parameters can be found in Table 1. The excitation was performed with a Tilted Optimized Non-saturating Excitation (TONE) pulse (Atkinson et al., 1994; Geurts et al., 2018), and the flip angle increased from 50 to 90° in the feet-head direction. A turbo field echo factor of 2 was used, to acquire two velocity encoding cycles per acquired time point in the cardiac cycle. This resulted in an acquired temporal resolution of 114 ms (57 ms reconstructed through interpolation). To

Fig. 1. Slice planning for the 2D phase contrast sequences. The left image shows the planning of the BG slice (in red) and the CSO slice (in green) on a sagittal T1 weighted image. The BG slice touches the underside of the corpus callosum, indicated by the dashed circles. The CSO slice is planned parallel to the BG slice and positioned 15 mm above the corpus callosum (Geurts et al., 2018). The center and right images show the planning of the MCA (in blue) on transverse and coronal T1 weighted images, respectively.

Table 1
Scanning parameters.

Parameter	CSO, BG	MCA	T1w
FOV (mm)	250×250	250×250	$300 \times 249 \times 190$
Slices	1	1	190
Voxel size (mm)	$0.3 \times 0.3 \times 2.0$	$0.5 \times 0.5 \times 2.5$	$1.0 \times 1.0 \times 1.0$
Flip angle (°)	50–90[a]	60	7
Venc (cm/s)	4, 20	100	–
TR/TE (ms)	28/16	8.5/5.4	4.1/2.0
BW (Hz/pix)	59	636	405
TFE factor	2	6	600[c]
Sense factor	1.5 (AP)	2 (AP)	2×2 (APxRL)
Shot interval (ms)	114	102	3 000
Time points	15	15	–
Scan time (min:s)[b]	5:37	0:51	0:45

[a] Increasing flip angle across the slice in the flow direction, using TONE (Atkinson et al., 1994).

[b] Listed scan times are given for the subject with the lowest heart rate (50 bpm, subject 5) and assume 100% scan efficiency (no RR-intervals rejected, true for subject 5). These are the longest scan times and therefore the longest breathing challenges.

[c] Thirty percent of the data (at the corners of k-space) was not acquired, yielding a complete T1w acquisition in 15 shots.

avoid phase wrapping, the encoding velocity was 4 cm/s for the CSO, 20 cm/s for the BG and 100 cm/s for the MCA. These encoding velocities have been empirically determined in previous studies (Bouvy et al., 2016; Geurts et al., 2018). The phase contrast acquisition through the MCA was slightly altered to be faster, since the MCA has larger dimensions and MCA blood signal has higher SNR.
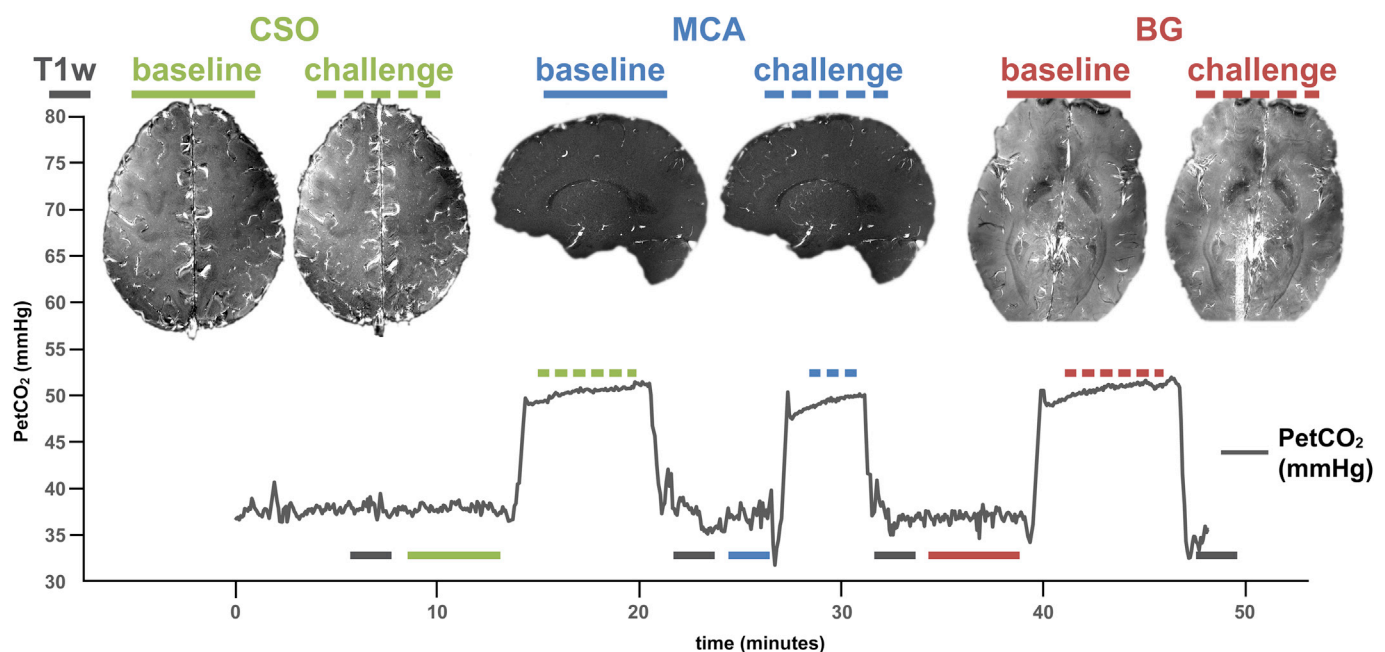
Breathing protocol

The CO_2 challenges were delivered using a computer-controlled gas blender and sequential gas delivery system running a feed-forward algorithm (RespirAct™, Thornhill Research Inc.). The $PetCO_2$ was recorded during each acquisition. A test run was performed outside of the MR suite to evaluate subject CO_2 tolerance. A schematic of the breathing protocol is shown in Fig. 2. Targeted $PetCO_2$ levels are reached within several breaths and reflect arterial partial pressure closely when using the

Respiract™ apparatus (Ito et al., 2008; Mark et al., 2010). The quick transitions from baseline to hypercapnia and vice versa can also be seen in Fig. 2. Each of the phase contrast acquisitions was performed twice; once during normal breathing at the individual baseline $PetCO_2$ and once with a challenge $PetCO_2$ targeted at an increase of 12 mmHg. Challenge duration depended on the heart rate-dependent acquisition duration, and ranged between 3 and 5.5 min.

Image processing

An in-house developed MATLAB (2015b, Mathworks) tool was used for data processing of the CSO and BG acquisitions (Geurts et al., 2018). Matlab functions from SPM (Wellcome Trust Centre for Neuroimaging) were used for white matter segmentation on the T1w image that was acquired closest in time to the phase contrast scan being analyzed. The resulting tissue probability map was transformed to the CSO slice and converted to a mask (threshold value 0.95 for white matter) to create a region of interest. For the BG slice the user manually selected the region of interest, which was bordered by the grey matter of the insula and the edges of the ventricles. The user annotated regions with pulsation artefacts in the stimulus acquisition (these were prone to artefacts due to hyperventilation and/or subject motion caused by the hypercapnic stimulus), these regions were excluded from analysis for both baseline and stimulus acquisitions.

Data within the regions of interest were corrected and processed to detect perforators, as previously described (Geurts et al., 2018). In short, background phase errors were removed with a median filter. Then, the standard deviation of noise was estimated from the complex signal of tissue over the cardiac cycle, which was used to calculate the 95% confidence interval of the mean velocity map. All voxels with significant velocity were labeled as a perforator. Only the voxel with the highest mean velocity was labeled if a group of directly adjacent voxels were significant, since perforators are at most one voxel in diameter. This resulted in a number of detected perforators ($N_{detected}$), each with a mean velocity during the cardiac cycle (V_{mean}). To find perforators that were detected during both baseline and stimulus, perforators were matched between the two acquisitions. Every identified perforator in one

Fig. 2. Breathing protocol. The graph shows the $PetCO_2$ trace for subject 5, with color coded lines representing each acquisition. The images on top are the actual mean magnitude images of each phase contrast measurement for this subject, in the order in which they were acquired. The color coded lines schematically indicate at which position on the trace they were acquired. The solid lines indicate baseline acquisitions and the dashed lines indicate challenge acquisitions. The phase contrast measurements were alternated with T1w acquisitions, which are indicated with a solid grey line.
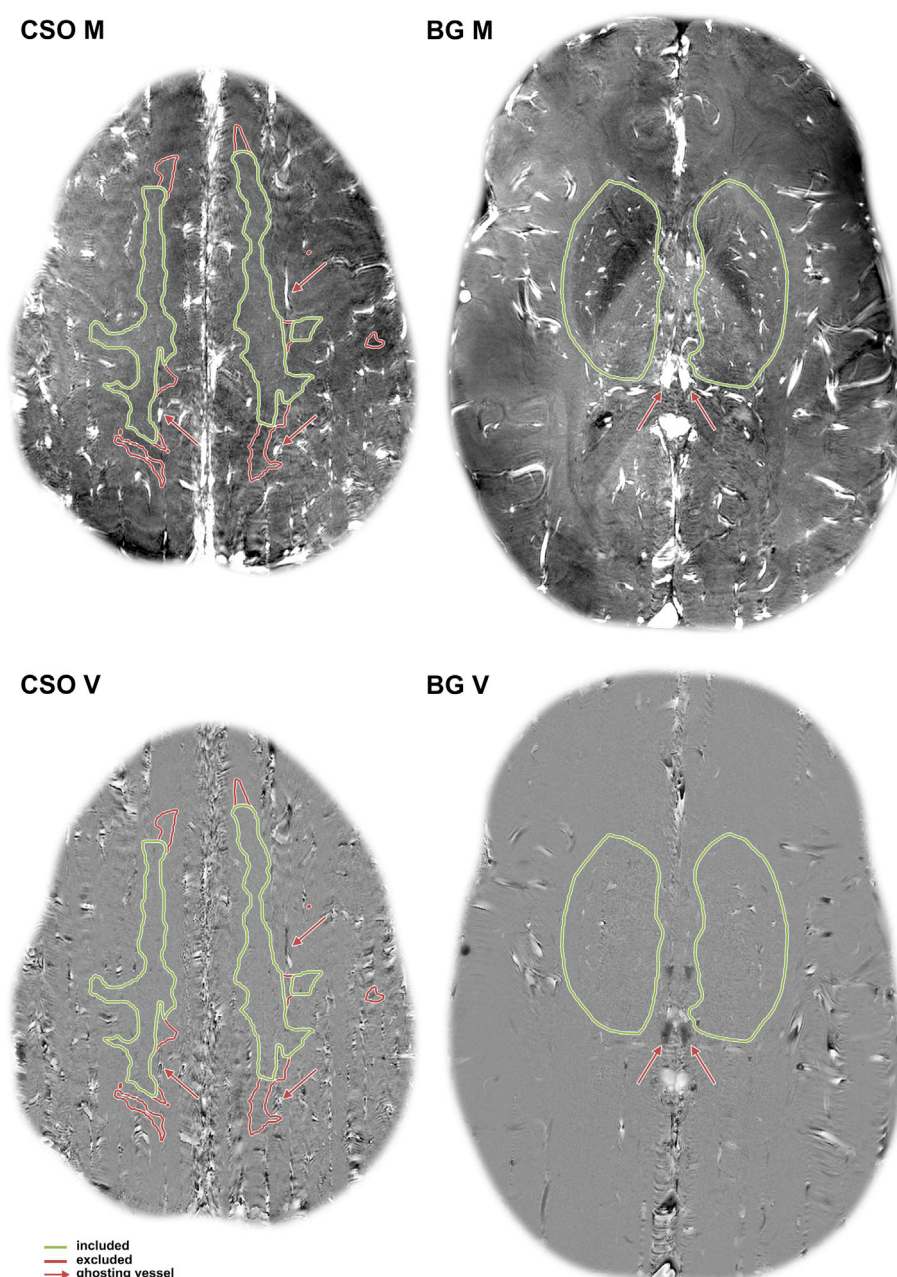
acquisition was matched to the perforator in the other acquisition that had the smallest distance to it, within 2 mm. Only the subgroup of perforators that were detected twice and matched between both acquisitions could be used to calculate reactivity. The processing of the MCA data was performed in a separate MATLAB tool, where the user selected a region of interest closely around the lumen of the MCA. Phase wraps present in the temporal curves of a voxel were unwrapped in the time domain by the MATLAB unwrap function. The total flow through the selected region in the MCA was calculated by averaging over time points and integrating over voxels.

Statistical analysis

Velocity reactivity (R_v) in the CSO and BG was calculated with a linear mixed effects (LME) model. We chose this since the velocity data had multiple levels (group and subject), and an ordinary least squares approach would have overestimated the confidence, since within-subject perforators are not independent from one another (Hox et al., 2010; Lindstrom and Bates, 1988; Laird and Ware, 1982). The model was set to explain the change in V_{mean} with the change in PetCO$_2$, the fitted slope being the parameter of interest ($R_v = \frac{\partial V}{\partial PetCO_2}$). R_v was converted to % change from baseline velocity after the fit. The LME model fits both a group effect and an effect per subject, allowing a portion of the variance to be explained explicitly by between subject differences, decreasing the residuals. It also allows the use of every detected perforator separately without averaging per subject, increasing the degrees of freedom (Hox et al., 2010; Lindstrom and Bates, 1988; Laird and Ware, 1982). The LME model was fitted and tested for significance with the NLME package (R Core Team) in R (R Foundation for Statistical Computing).

Since the MCA data consists of only the subject level, the LME model collapses to ordinary least squares. Therefore, the flow reactivity (R_φ) of the MCA was determined using an ordinary least squares approach. MATLAB was used to test R_φ for significance. The measured flow was taken as the input measurement and the measured PetCO$_2$ was taken as

CSO M   **BG M**

CSO V   **BG V**

— included
— excluded
→ ghosting vessel

Fig. 3. Manual region of interest adjustments. These images show the mean magnitude (M, top row) and velocity (V, bottom row) data of 2D phase contrast acquisitions of mediocre quality, in which pulsation artefacts had to be excluded. The pulsation artefacts show up as vertical lines (in the phase encoding direction) of repetitions of the originating vessel. At these locations the data is corrupted and has to be excluded. The left image shows a CSO slice in which the automatically segmented ROI contained pulsation artefacts from surrounding vessels (red arrows). The red lines show ROI portions that were manually removed, the green lines show the remaining ROI that was included. The right image shows a BG slice in which pulsation artefacts from surrounding vessels (red arrows) had to be avoided during manual segmentation (green lines).

regressor. The fitted slope, converted to % change from baseline flow, was taken as the measure for flow reactivity.

Changes in $N_{detected}$ were tested for significance using paired Student's t-tests. For this study, a probability for type I errors (α) smaller than 0.05 was decided to be significant. The change in $N_{detected}$ was tested single-sided.

Simulations

We simulated the 2D phase contrast measurement of velocity and CVR using the Bloch equations. Because only some simulation boundary conditions are known for cerebral perforating arteries in humans, several assumptions on similarity to other vessels and species were made. This limited our interpretation to qualitative statements. Due to the nature of these limitations, and not to distract from the main findings of the study, we supply the simulations in appendix A for the interested reader.

Results

Included subjects (mean age ± standard deviation, SD: 26 ± 5 years, 5 females) had individual $PetCO_2$ baselines of (mean ± SD) 36.4 ± 1.6 mmHg, and achieved increases of 12.0 ± 2.1 mmHg during challenges. CSO acquisitions were successfully completed in all ten subjects, however one CSO challenge measurement was repeated due to excessive motion artefacts. Two BG challenge acquisitions were excluded because of motion artefacts, yielding eight successfully completed BG acquisitions. One MCA challenge acquisition was excluded because of motion artefacts, yielding nine successful acquisitions. Fig. 3 shows the included region of interest for a subject that showed some motion artefacts.

With the applied technique we could indeed measure vascular reactivity, also in the smallest perforators in the CSO. We observed that the CO_2 challenge not only increased the flow velocity, but also the number of CSO perforators that was detected. Fig. 4 shows all velocity measurements and fitted reactivities. The measured R_v (fit ± standard error) was 0.7 ± 0.3%/mmHg in the CSO ($P < 0.01$) and 1.6 ± 0.5%/mmHg in the BG ($P < 0.001$). The measured R_φ in the MCA was 5.2 ± 1.4%/mmHg
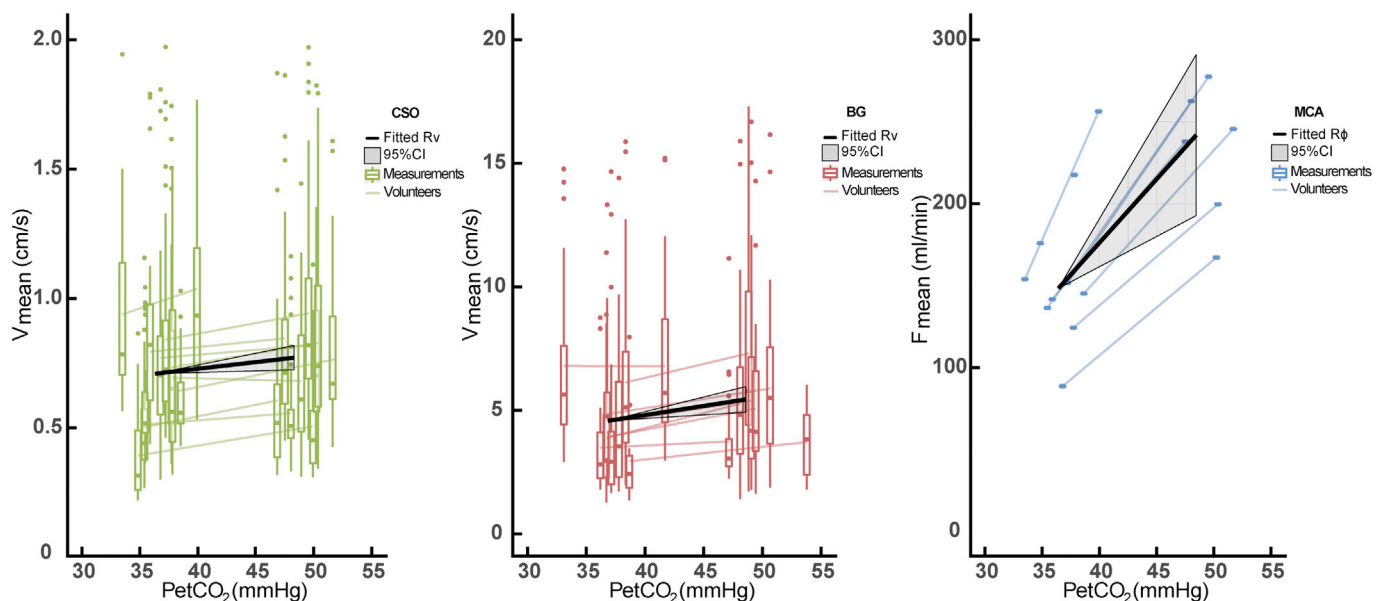
($P < 0.01$). Visual inspection of phase contrast acquisitions showed more apparent perforators during challenge than during baseline (see Fig. 5). The number of detected perforators showed an increase from baseline to hypercapnic challenge for all subjects and acquisitions, except in one BG set. The number (mean [range]) increased from 63 [27–88] to 108 [61–178] in the CSO ($P < 0.001$) and from 48 [24–66] to 63 [32–91] in the BG ($P < 0.01$) (see Fig. 6). The number of detected vessels in the subset that were detected twice and matched between baseline and challenge (mean [range]) was 39 [20–80] for the CSO and 33 [13–46] for the BG.

Simulation qualitatively showed that the 2D phase contrast assessment of velocity reactivity in perforating arteries can be an overestimation, depending on perforator diameters, as can be seen in Figure A.1 of appendix A. The overestimation in reactivity as function of perforator diameter in the CSO was estimated to be -0.01%/mmHg/μm, implying less overestimation for larger diameters. The overestimation would be 0.04%/mmHg higher in hypertensive patients, who typically have lower reactivity than healthy controls. The systematic error vanished as vessel diameters approached the acquired voxel size, as is likely the case in the BG. High blood flow velocity and tissue signal saturation also decreased overestimation. For complete results of the simulation we refer to appendix A.

Discussion

Small vessel specific reactivity was successfully measured in cerebral perforating arteries of the CSO and BG, using 2D phase contrast at 7 T. Significant velocity reactivity was measured in both the CSO and the BG. In both the CSO and the BG the number of detected vessels increased significantly and consistently during the breathing challenge, reflecting increased blood flow through the T1-inflow effect. Thus, the number of detected vessels can be considered as an additional measure for reactivity. These results show the feasibility of measuring CVR specifically on the arterial side of the microcirculation of cerebral white matter and the basal ganglia.

The measured velocity reactivity in the CSO and BG of 0.7 and 1.6%/mmHg, respectively, are in the same range as reactivity reported with
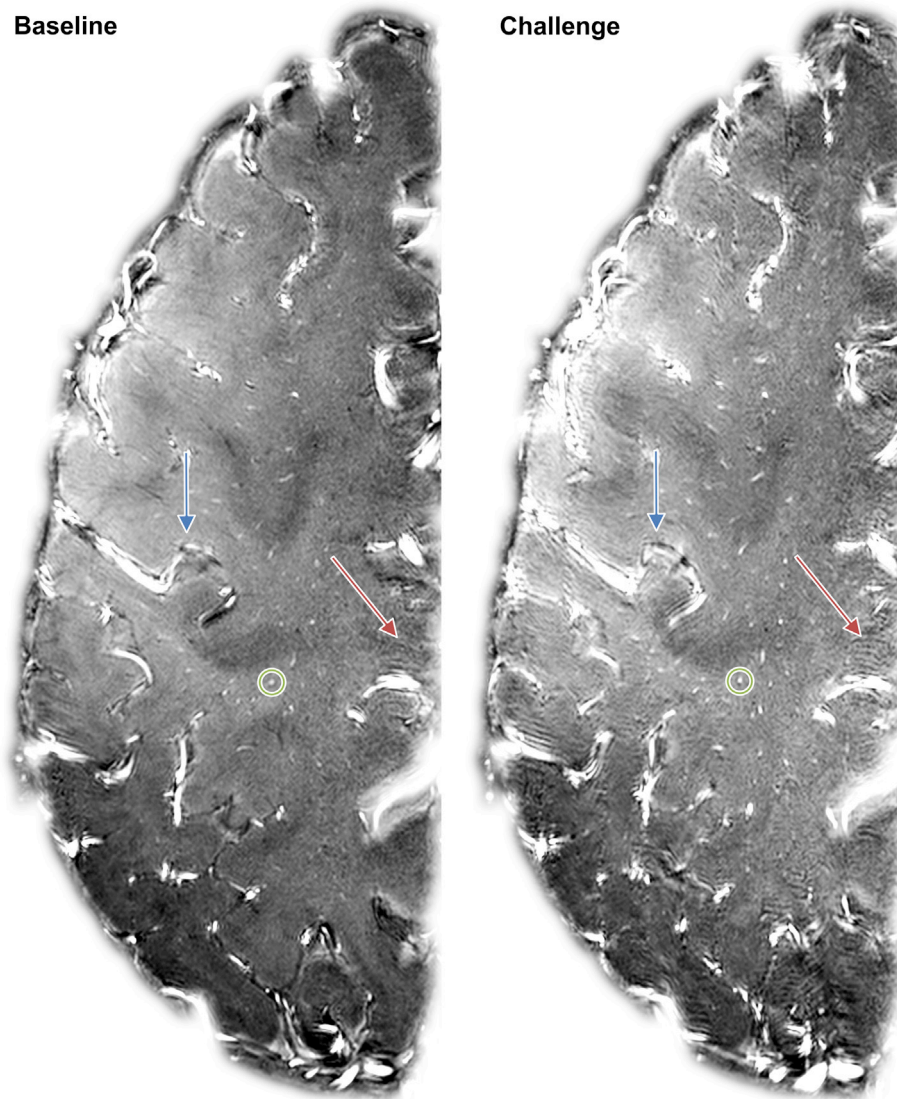

Fig. 4. Measured velocities and fitted reactivity. These plots show a colored boxplot for the vessels that could be matched between baseline and challenge measurements, for each scan of each subject. The boxplots corresponding to the same volunteer are connected with a colored line, representing the individual fit. The fitted reactivity for all subjects is shown in black, with the 95% CI in grey. The horizontal axes show $PetCO_2$ and the vertical axes show the measured quantity, which is mean flow (F_{mean}) for the MCA and mean velocity (V_{mean}) for the BG and the CSO. The left, middle and right graphs show the results for the CSO (green), BG (red) and MCA (blue) measurements respectively. Note that attained $PetCO_2$ values are nearly identical between experiments, both for baseline and challenge measurements.
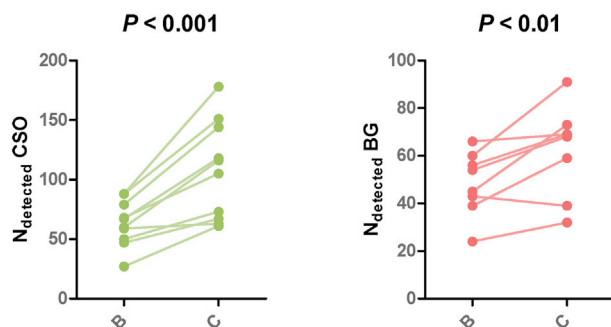
Baseline

Challenge

Fig. 5. Mean magnitude at baseline and during challenge. The left image shows the mean CSO magnitude of the right hemisphere of subject 5 at baseline and the right image shows the same during challenge. Note the higher blood signal on the right image during the hypercapnic breathing challenge, which caused a larger number of perforators to be detected during the challenge acquisitions. The increase in blood signal is caused by an increase in flow and the T1-inflow effect. The green circles show one example of an included perforator, which was located in the white matter, was not corrupted by ghosting during challenge, and was detected in both acquisitions. The blue arrows points at a curved sulcus with intra-sulcal vessels running through. These sulci and surrounding gray matter were automatically excluded. The red arrows show an area with a ghosting artefact of an intra-sulcal vessel during the challenge acquisition. These areas with ghosting artefacts during challenge were manually annotated and excluded from both acquisitions. The images are masked and scaled identically.

Fig. 6. Number of detected perforators. The markers show the number of detected perforators at baseline (B) and the round markers show those during challenge (C). Corresponding subjects are denoted with solid lines. The left graph shows the results for the CSO measurements (green), the right graph shows the results for the BG measurements (red).

ASL. While ASL reflects flow and not velocity, Mandell et al. assessed reactivity using ASL, and reported a comparable CVR of 0.5%/mmHg and 1.5%/mmHg in white and grey matter, respectively (Mandell et al., 2008). Bhogal et al. assessed reactivity with BOLD, and reported a lower

CVR of 0.21%/mmHg and 0.40%/mmHg in white and grey matter, respectively (Bhogal et al., 2015). However, reactivity as measured by BOLD is influenced by scan parameters and blood flow, volume and oxygenation, which hampers a direct comparison. Human retinal arteriolar velocity reactivity has been measured to be 1.7%/mmHg with Doppler laser velocimetry, which also falls in the same range of reactivity values (Rose et al., 2014; Tayyari et al., 2017; Venkataraman et al., 2017). The measured reactivity of the MCA corresponds well to reactivity values measured in the MCA with Doppler ultrasound and phase contrast MRI as found in literature (Leung et al., 2013; Madureira et al., 2017; Valdueza et al., 1999).

The secondary outcome $N_{detected}$ turned out to be very sensitive to PetCO$_2$ changes, which might be of use for studies with small effect sizes. A change in $N_{detected}$ indicates a change in flow, since $N_{detected}$ depends on SNR and the SNR of blood depends in the T1 inflow effect. Not all perforators were detected again during the challenge acquisition. On average 39 out of 63 perforators in the CSO and 33 out of 48 in the BG were detected twice. Since the small perforators in this study are just within our ability to detect, each repeated measurement might detect a slightly different set by chance. Small changes in physiology or subject position might also cause perforators to move in- and out of the detection limit. Besides that, there might be some false positive detections that explain a part of these differences.

It should be noted that no reactivity measurements of the perforators have been performed as yet, preventing direct comparisons with reference values. To address this issue we performed simulations which qualitatively show that our measurement might overestimate reactivity. This effect is most pronounced if perforator diameters are much smaller than voxel dimensions and if tissue signal is poorly suppressed. We estimated that the velocity reactivity would be overestimated more in hypertensive patients than in healthy controls by 0.04%/mmHg in the CSO, while this difference in overestimation would approach zero in the BG. In other words, reactivity is overestimated more in subjects with smaller vessels. Since patients are generally expected to have smaller vessels and lower reactivity, if a study does detect a lower reactivity in patients relative to controls despite the opposite systematic error, it is likely to be true. This does leave an ambiguity of the results if a higher reactivity is detected in patients or when patients are investigated that have larger vessels than controls, which makes the results less specific in such cases. These effects are most likely negligible when measuring reactivity in the BG.

The method demonstrated in this paper complements existing CVR measurements by allowing reactivity measurements directly at the level of the perforators. Assessing CVR in-between the currently measured level of the large arteries or the tissue level, can help understand reactivity across the entire cerebrovascular network. Another location aspect is that the presented method, like ASL, measures at the arterial side of the vasculature, since venous blood (with a short T2* of about 6 ms at 7 T) (Yacoub et al., 2001) will have lost most of its signal at the chosen TE (Geurts et al., 2018; Yacoub et al., 2001). This is in contrast to BOLD MRI which mainly reflects venous blood hemodynamics. The method is also able to measure reactivity in white matter using just tens of perforators, which can complement the low SNR that ASL and BOLD reactivity studies show for white matter (Bhogal et al., 2015; Sam et al., 2016b). Besides the location, it has the feature of measuring a single physical quantity, without the need for a model or being dependent on boundary condition assumptions. On one hand this complements BOLD measurements of CVR, since BOLD reactivity is a compound hemodynamic effect. On the other hand this also complements ASL measurements of CVR, since ASL depends on fitting a kinetic model with various assumptions (Buxton et al., 1998). Like ASL and BOLD measurements of CVR, the presented method is user independent. We think that because of these combined attributes, the method can help explore unknown terrain.

The study has some limitations. First, the voxels that we identify as perforators have a partial volume effect between blood signal and tissue signal. This is caused by tissue spins that are not fully saturated and by sub-voxel perforator diameters. The partial volume effect leads to an underestimation of the measured velocities. The simulations from the appendix suggest that this leads to an overestimation of the reactivity. Because the true diameters and diameter changes in response to increased PetCO$_2$ are unknown, it is not possible to determine the exact amount of reactivity overestimation. As a further limitation, the presented method assesses changes in velocity instead of flow. However, studies have shown that velocity does increase under vasodilatory stimulus in vessels both larger and smaller than the perforators in this study (Leung et al., 2013; Rose et al., 2014; Venkataraman et al., 2017). Like flow reactivity, a decreased velocity reactivity is correlated with cerebrovascular disease (Klijn et al., 2000; Rose et al., 2014; Stevenson et al., 2010; Venkataraman et al., 2017; Vicenzini et al., 2007). Besides these limitations, increasing the PetCO$_2$ is uncomfortable and can increase the breathing and heart rate of subjects, potentially translating into motion artefacts. Pulsation artefacts also worsen, which increase the ghosting of sulcal arteries into tissue. The current method is susceptible to motion artefacts because of the small voxel size and the small perforators that are imaged. The artefacts caused by within acquisition motion led to the corruption of three CSO/BG scans. Motion between baseline and challenge was less detrimental and led to only a subset of perforators being detected in both acquisitions, which was still a sizable group. The current method, like other high resolution applications, would benefit

greatly from new motion correction methods (Stucht et al., 2015). We limited the influence of motion artefacts by excluding acquisitions with severe motion artefacts and by excluding voxels with ghosting artefacts. Subject motion might be worse in patient groups, in which case in-plane registration can be considered to alleviate a part of the problem. A final limitation relates to cerebral perforators that were not perfectly perpendicular to the single imaging slice. This issue is partially alleviated due to anatomy, since perforators in the CSO run more or less vertically from the gyri in a central direction. Moreover, angulation of a perforator has only limited influence on the calculation of reactivity. The angulation of a perforator reduces the measured velocity, however this is present during both the baseline and challenge measurements, which causes it to divide out when calculating the percentage velocity increase. Finally, a perforator that runs oblique to the imaging slice has a smaller chance of being detected due to SNR reducing partial volume effects associated with the large slice thickness and small in-plane voxel size.

Conclusion

We have shown that 2D phase contrast at 7 T is able to measure velocity reactivity in cerebral perforating arteries of different sizes. These arteries are of special interest as they are involved in various cerebrovascular diseases. The results correspond well to literature values obtained with various other methods. With the contribution of this work it is now possible for future studies to assess small vessel specific reactivity.

Conflicts of interest

None.

Acknowledgements

Appendix A. Supplementary data

Supplementary data related to this article can be found at https://doi.org/10.1016/j.neuroimage.2018.01.055.

References

Atkinson, D., Brant-Zawadzki, M., Gillan, G., Purdy, D., Laub, G., 1994. Improved MR angiography: magnetization transfer suppression with variable flip angle excitation and increased resolution. Radiology 190, 890–894. https://doi.org/10.1148/radiology.190.3.8115646.

Beishon, L., Haunton, V.J., Panerai, R.B., Robinson, T.G., 2017. Cerebral hemodynamics in mild cognitive Impairment . Syst. Rev. 59, 369–385. https://doi.org/10.3233/JAD-170181.

Bhogal, A.A., Siero, J.C.W., Fisher, J.A., Froeling, M., Luijten, P., Philippens, M., Hoogduin, H., 2014. Investigating the non-linearity of the BOLD cerebrovascular reactivity response to targeted hypo/hypercapnia at 7T. Neuroimage 98, 296–305. https://doi.org/10.1016/j.neuroimage.2014.05.006.

Bhogal, A.A., Philippens, M.E.P., Siero, J.C.W., Fisher, J.A., Thade, E., Luijten, P.R., Hoogduin, H., 2015. NeuroImage Examining the regional and cerebral depth-dependent BOLD cerebrovascular reactivity response at 7 T. Neuroimage 114, 239–248. https://doi.org/10.1016/j.neuroimage.2015.04.014.

Bouvy, W.H., Geurts, L.J., Kuijf, H.J., Luijten, P.R., Kappelle, L.J., Biessels, G.J., Zwanenburg, J.J., 2016. Assessment of Blood Flow Velocity and Pulsatility in Cerebral Perforating Arteries with 7-T Quantitative Flow MRI. https://doi.org/10.1002/nbm.3306.

Broderick, J.P., Brott, T.G., Kothari, R., Miller, R., Mills, D., Minneci, L., Khoury, J., 1997. Incidence rates of ischemic stroke and stroke subtypes among blacks. Neurology 48, 7003.

Brown, R. w., cheng, Y. n., Haacke, M. e., Thompson, michael R., Venkatesan, R., 2014. Magnetic Resonance Imaging: Physical Principles and Sequence Design, second ed. Wiley Blackwell. https://doi.org/10.1002/9781118633953.

Buxton, R.B., Frank, L.R., Wong, E.C., Siewert, B., Warach, S., Edelman, R.R., 1998. A general kinetic model for quantitative perfusion imaging with arterial spin labeling. Magn. Reson. Med. 40, 383–396. https://doi.org/10.1002/mrm.1910400308.

Geurts, L., Biessels, G.J., Luijten, P., Zwanenburg, J., 2018. Better and faster velocity pulsatility assessment in cerebral white matter perforating arteries with 7T quantitative flow MRI through improved slice profile, acquisition scheme, and postprocessing. Magn. Reson. Med. ISSN: 1522-2594 79 (3), 1473–1482. https://doi.org/10.1002/mrm.26821.

Halani, S., Kwinta, J.B., Golestani, A.M., Khatamian, Y.B., Chen, J.J., 2015. Comparing cerebrovascular reactivity measured using BOLD and cerebral blood flow MRI: the effect of basal vascular tension on vasodilatory and vasoconstrictive reactivity. Neuroimage 110, 110–123. https://doi.org/10.1016/j.neuroimage.2015.01.050.

Reuck, J. De, Decoo, D., Hasenbroekx, M.C., Lamont, B., Santens, P., 1999. Acetazolamide Vasoreactivity in Vascular Dementia : a Positron Emission Tomographic Study, pp. 31–36.

Heijtel, D.F.R., Mutsaerts, H.J.M.M., Bakker, E., Schober, P., Stevens, M.F., Petersen, E.T., Berckel, B.N.M., Van Majoie, C.B.L.M., Booij, J., Osch, M.J.P., Van Boellaard, R., Lammertsma, A.A., Nederveen, A.J., 2014. NeuroImage Accuracy and precision of pseudo-continuous arterial spin labeling perfusion during baseline and hypercapnia : a head-to-head comparison with 15 O H 2 O positron emission tomography. Neuroimage 92, 182–192. https://doi.org/10.1016/j.neuroimage.2014.02.011.

Hox, J.J., Moerbeek, M., van de Schoot, R., 2010. Multilevel Analysis: Techniques and Applications, second ed. Lawrence Erlbaum Associates Inc.

Ito, S., Mardimae, A., Han, J., Duffin, J., Wells, G., Fedorko, L., Minkovich, L., Katznelson, R., Meineri, M., Arenovich, T., Kessler, C., Fisher, J.A., 2008. Non-invasive prospective targeting of arterial P CO 2 in subjects at rest. J. Physiol. 586, 3675–3682. https://doi.org/10.1113/jphysiol.2008.154716.

Klijn, C.J., Kappelle, L.J., van Huffelen, a C., Visser, G.H., Algra, a, Tulleken, C. a, van Gijn, J., 2000. Recurrent ischemia in symptomatic carotid occlusion: prognostic value of hemodynamic factors. Neurology 55, 1806–1812. https://doi.org/10.1212/WNL.57.1.161-a.

Laird, N.M., Ware, J.H., 1982. Random-effects models for longitudinal data. Int. Biometric Soc. 38, 963–974.

Lee, K., Lee, K., Lee, S., Ahn, C., Park, J.S., 2007. Lacunar Infarction in Type 2 Diabetes Is Associated with an Elevated Intracranial Arterial Pulsatility Index, vol. 48, pp. 802–806. https://doi.org/10.3349/ymj.2007.48.5.802.

Leung, J., Behpour, A., Sokol, N., Mohanta, A., Kassner, A., 2013. Assessment of Intracranial Blood Flow Velocities Using a Computer Controlled Vasoactive Stimulus ;: A Comparison Between Phase Contrast Magnetic Resonance Angiography and Transcranial Doppler Ultrasonography, vol. 738, pp. 733–738. https://doi.org/10.1002/jmri.23911.

Lindstrom, M.J., Bates, D.M., 1988. Newton-Raphson and EM algorithms for linear mixed-effects models for repeated measures data. J. Am. Stat. Assoc. 83, 1014–1022. https://doi.org/10.2307/2290128.

Madureira, J., Castro, P., Azevedo, E., 2017. Demographic and systemic hemodynamic influences in mechanisms of cerebrovascular regulation in healthy adults. J. Stroke Cerebrovasc. Dis. 26, 500–508. https://doi.org/10.1016/j.jstrokecerebrovasdis.2016.12.003.

Mandell, D.M., Han, J.S., Poublanc, J., Crawley, A.P., Kassner, A., Fisher, J.A., Mikulis, D.J., 2008. Selective reduction of blood flow to white matter during hypercapnia corresponds with leukoaraiosis. Stroke 39, 1993–1998. https://doi.org/10.1161/STROKEAHA.107.501692.

Mark, C.I., Slessarev, M., Ito, S., Han, J., Fisher, J.A., Pike, G.B., 2010. Precise control of end-tidal carbon dioxide and oxygen improves BOLD and ASL cerebrovascular reactivity measures. Magn. Reson. Med. 64, 749–756. https://doi.org/10.1002/mrm.22405.

Mitchell, G.F., 2008. Effects of central arterial aging on the structure and function of the peripheral vasculature: implications for end-organ damage. J. Appl. Physiol. 105, 1652–1660. https://doi.org/10.1152/japplphysiol.90549.2008.

Mitchell, G.F., Van Buchem, M.A., Sigurdsson, S., Gotal, J.D., Jonsdottir, M.K., Kjartansson, Ó lafur, Garcia, M., Aspelund, T., Harris, T.B., Gudnason, V.,

Launer, L.J., 2011. Arterial stiffness, pressure and flow pulsatility and brain structure and function: the Age, Gene/Environment Susceptibility-Reykjavik Study. Brain 134, 3398–3407. https://doi.org/10.1093/brain/awr253.

Pantoni, L., 2010. Cerebral small vessel disease: from pathogenesis and clinical characteristics to therapeutic challenges. Lancet Neurol. 9, 689–701. https://doi.org/10.1016/S1474-4422(10)70104-6.

Reinhard, M., Schwarzer, G., Briel, M., Altamura, C., Palazzo, P., King, A., Bornstein, N.M., Petersen, N., Motschall, E., Hetzel, A., Marshall, R.S., Klijn, C.J.M., Silvestrini, M., Markus, H.S., Vernieri, F., 2014. Cerebrovascular reactivity predicts stroke in high-grade carotid artery disease. Neurology 83, 1424–1431. https://doi.org/10.1212/WNL.0000000000000888.

Rose, K., Flanagan, J.G., Patel, S.R., Cheng, R., Hudson, C., 2014. Retinal blood flow and vascular reactivity in chronic smokers. Investig. Ophthalmol. Vis. Sci. 55, 4266–4275. https://doi.org/10.1167/iovs.14-14022.

Sam, K., Conklin, J., Holmes, K.R., Sobczyk, O., Poublanc, J., Crawley, A.P., Mandell, D.M., Venkatraghavan, L., Duf, J., Fisher, J.A., Black, S.E., Mikulis, D.J., 2016a. NeuroImage ;: Clinical Impaired Dynamic Cerebrovascular Response to Hypercapnia Predicts Development of White Matter Hyperintensities, vol. 11, pp. 796–801. https://doi.org/10.1016/j.nicl.2016.05.008.

Sam, K., Crawley, A.P., Conklin, J., Poublanc, J., Sobczyk, O., Mandell, D.M., Venkatraghavan, L., Duffin, J., Fisher, J.A., Black, S.E., Mikulis, D.J., 2016b. Development of White Matter Hyperintensity Is Preceded by Reduced Cerebrovascular Reactivity, pp. 277–285. https://doi.org/10.1002/ana.24712.

Stevenson, S.F., Doubal, F.N., Shuler, K., Wardlaw, J.M., 2010. A systematic review of dynamic cerebral and peripheral endothelial function in lacunar stroke versus controls. Stroke 41, 434–443. https://doi.org/10.1161/STROKEAHA.109.569855.

Stucht, D., Danishad, K.A., Schulze, P., Godenschweger, F., Zaitsev, M., Speck, O., 2015. Highest resolution in vivo human brain MRI using prospective motion correction. PLoS One 10, 1–17. https://doi.org/10.1371/journal.pone.0133921.

Tayyari, F., Venkataraman, S.T., Gilmore, E.D., Wong, T., Fisher, J., Hudson, C., 2017. The Relationship between Retinal Vascular Reactivity and Arteriolar Diameter in Response to Metabolic Provocation, vol. 50, pp. 4814–4821. https://doi.org/10.1167/iovs.09-3373.

Valdueza, J.M., Draganski, B., Hoffmann, O., Dirnagl, U., Einhäupl, K.M., 1999. Analysis of CO2 vasomotor reactivity and vessel diameter changes by simultaneous venous and arterial Doppler recordings. Stroke 30, 81–86. https://doi.org/10.1161/01.STR.30.1.81.

Venkataraman, S.T., Hudson, C., Rachmiel, R., Buys, Y.M., Markowitz, S.N., Fisher, J.A., Trope, G.E., Flanagan, J.G., 2017. Retinal Arteriolar Vascular Reactivity in Untreated and Progressive Primary Open-angle Glaucoma, vol. 51. https://doi.org/10.1167/iovs.09-3630.

Verbree, J., Bronzwaer, A.G.T., Ghariq, E., Versluis, M.J., Daemen, M.J.A.P., Buchem, M.A. Van, Dahan, A., Lieshout, J.J. Van, Osch, M.J.P. Van, 2014. Assessment of Middle Cerebral Artery Diameter during Hypocapnia and Hypercapnia in Humans Using Ultra-high-field MRI, pp. 1084–1089. https://doi.org/10.1152/japplphysiol.00651.2014.

Vicenzini, E., Chiara, M., Marta, R., Francesco, A., 2007. . Cerebrovascular Reactivity in Degenerative and Vascular Dementia ;: a Transcranial Doppler Study, pp. 84–89. https://doi.org/10.1159/000103642.

Wardlaw, J.M., Smith, E.E., Biessels, G.J., Cordonnier, C., Fazekas, F., Frayne, R., Lindley, R.I., O'Brien, J.T., Barkhof, F., Benavente, O.R., Black, S.E., Brayne, C., Breteler, M., Chabriat, H., DeCarli, C., de Leeuw, F.E., Doubal, F., Duering, M., Fox, N.C., Greenberg, S., Hachinski, V., Kilimann, I., Mok, V., Oostenbrugge, R., Van Pantoni, L., Speck, O., Stephan, B.C.M., Teipel, S., Viswanathan, A., Werring, D., Chen, C., Smith, C., van Buchem, M., Norrving, B., Gorelick, P.B., Dichgans, M., 2013. Neuroimaging standards for research into small vessel disease and its contribution to ageing and neurodegeneration. Lancet Neurol. 12, 822–838. https://doi.org/10.1016/S1474-4422(13)70124-8.

Yacoub, E., Shmuel, A., Pfeuffer, J., Moortele, P., Van De Adriany, G., Andersen, P., Vaughan, J.T., Merkle, H., Ugurbil, K., 2001. Imaging Brain Function in Humans at 7 Tesla, pp. 588–594.